Biochemical and Biophysical Research Communications 496 (2018) 529–535

Contents lists available at ScienceDirect

Biochemical and Biophysical Research Communications

journal homepage: www.elsevier.com/locate/ybbrc

Analysis of the interactions between GMF and Arp2/3 complex in two binding sites by molecular dynamics simulation

A. Popinako [a], M. Antonov [b], D. Dibrova [c], A. Chemeris [c], O.S. Sokolova [c, *]

[a] A.N. Bach Institute of Biochemistry, Research Center of Biotechnology of RAS, 33 Leninsky Ave, bld. 2, Moscow, 119071, Russia
[b] M.K. Ammosov North-Eastern Federal University, 58 Belinskiy str, suite 312, Yakutsk, 677980, Republic of Sakha (Yakutia), Russia
[c] Lomonosov Moscow State University, Faculty of Biology, 1 Leninskie gory, bld 12, Moscow, 119234, Russia

ARTICLE INFO

Article history:
Received 3 January 2018
Accepted 11 January 2018
Available online 12 January 2018

Keywords:
Arp2/3 complex
GMF
Crystal structure
Single particle electron microscopy
Molecular modeling
Inactivation

ABSTRACT

The Arp2/3 complex plays a key role in nucleating actin filaments branching. The glia maturation factor (GMF) competes with activators for interacting with the Arp2/3 complex and initiates the debranching of actin filaments. In this study, we performed a comparative analysis of interactions between GMF and the Arp2/3 complex and identified new amino acid residues involved in GMF binding to the Arp2/3 complex at two separate sites, revealed by X-ray and single particle EM techniques. Using molecular dynamics simulations we demonstrated the quantitative and qualitative changes in hydrogen bonds upon binding with GMF. We identified the specific amino acid residues in GMF and Arp2/3 complex that stabilize the interactions and estimated the mean force profile for the GMF using umbrella sampling. Phylogenetic and structural analyses of the recently defined GMF binding site on the Arp3 subunit indicate a new mechanism for Arp2/3 complex inactivation that involves interactions between the Arp2/3 complex and GMF at two binding sites.

1. Introduction

The Arp2/3 complex initiates branching of actin filaments [1]. It is thereby involved in the processes of cell migration, cytokinetics and intracellular transport. According to numerous studies, the change in actin dynamics is often closely associated with neoblastic transformation of cells [2].

The Arp2/3 complex consists of five subunits from ARPC1 to ARPC5 and two Actin Related Protein subunits: Arp2 and Arp3 (Fig. S1). Conformation changes in the Arp2/3 complex are regulated through the interactions with different factors (activators and inactivators). The activators/NPFs, including WASP, N-WASp and Scar/WAVE [3,4] all possess a VCA-domain on their C-termini, comprising of three short fragments: a V-motif (verprolin homology, also called WH2, WASp homolog 2), a C-motif (central or cofilin homology) and an A-motif (acidic) [5]. The Arp2/3 complex interacts with the VCA domain of WASp family proteins, the actin monomers and an actin filament during the formation of the branch [6]. In this complex, the V-motif binds to actin monomers at their pointed end [7]; the C-motif promotes the binding of VCA to actin monomers and to the Arp2/3 complex [8], and the A-motif binds to the Arp2/3 complex [9]. The free VCA domain is unstructured, but it obtains a secondary structure in contact with the Arp2/3 complex [10].

By homology with the NPFs, inactivators of the Arp2/3 complex have been discovered that compete with VCA for interacting with the Arp2/3 complex [1,11]. One of the inactivators, Glia Maturation Factor (GMF), is responsible for debranching of actin filaments [11]. Recently, the crystal structure of the Arp2/3 complex from *Bos taurus* with the GMF from *Mus musculus* was published, which revealed one binding site for GMF on the Arp2/3 complex, located near ARPC1 and Arp2 subunits [12] (site GMF-IX on Fig. S1).

Recent experiments, including analytical ultracentrifugation, cross-linking [13] and time-resolved FRET [10], suggested that more than one activator is required to completely activate the Arp2/3 complex. This may point to the fact that more than one inactivator is required as well [10,11,14]. A model of GMF-induced debranching of actin filaments has recently been proposed that includes two sites of interactions of Gmf1 with the Arp2/3 complex [11]. This model has recently been supported by our structural studies [14]. Two 3D structures of the Arp2/3 complex with Gmf1 were

Abbreviations: MD, molecular dynamics; NPF, nucleation-promoting factor; EM, electron microscopy.

* Corresponding author.
E-mail address: sokolova@mail.bio.msu.ru (O.S. Sokolova).

https://doi.org/10.1016/j.bbrc.2018.01.080
0006-291X/

obtained: one in a 'standard' open conformation [15] that has an additional mass attributed to Gmf1, close to the Arp2 subunit, and the other in a 'new' open conformation that indicated the presence of a second binding site for Gmf1 on the Arp2/3 complex, at the back of the Arp3 subunit (site GMG-IIEM on Fig. S1).

In this study, we performed a comparative MD analysis of interactions between GMF and the Arp2/3 complex in two binding sites, revealed by single particle EM and compared them to one site found by X-ray. We identified new amino acid residues involved in binding of GMF to the Arp2/3 complex and demonstrated that they are conserved throughout all homologues from evolutionarily distant species.

2. Methods

2.1. Modeling and structural analysis of the models

The model of the Arp2/3 complex with GMF, revealed by X-ray (further referred to as GMF-IX), has been downloaded from rscb.org (pdb id 4JD2 [12]). Two models of the Arp2/3 complex with GMF, revealed by single particle EM, were built based on our recently published EM density maps [14] and referred to as GMF-IEM (GMF positioned near Arp2/ARPC1 subunits) and GMF-IIEM (GMF positioned near Arp3 subunit). We used UCSF Chimera rigid body docking to fit the GMF (pdb id 4JD2, chain H) into the EM map [14]. The correlation coefficient was 0.95 before MD, calculated in UCSF Chimera.

The hydrophobic organization of interacting monomers in complexes was analyzed by Platinum web-service [16]. The contacts between the Arp2/3 complex and GMF were revealed using the Protein Interactions Calculator (PIC) server [17]. The binding affinity in protein-protein complexes was predicted using PRODIGY (PROtein binDIng enerGY prediction) webserver [18].

2.2. Bioinformatics analysis

GMF sequences were found from BLAST [19] searches against the representative sample of 84 eukaryotic genomes taken from NCBI's RefSeq database [20] (see Table S1 for complete list). The multiple alignment of GMF sequences was constructed with MUSCLE [21] and visualized using GeneDoc and Jalview editing [22]. Phylogenic trees were constructed with the MEGA 7 [23] using the JTT model of amino acids substitutions, with uniform rates and partial deletion of gapped regions at 80% presence threshold.

2.3. Molecular simulation

Molecular models of the Arp2/3 complex with GMF positioned in three binding sites were embedded in a water filled dodecahedron box, a minimum distance between periodic boundary images was 3.4 nm. Simulations were carried out using the GROMACS v4.6.5 package [24] with a OPLS-AA (optimized potentials for liquid simulations all atom) force field [25] and a TIP4P water model. All ionizable residues were set to their ionization states expected at pH 7.0. The total charge of the system was neutralized by the addition of 6 (for GMF-IX), 4 (for GMF-IIEM), 2 (for GMF-IEM) Na + ions. Before modeling, the system was optimized using the conjugate gradient method. The relaxation of the system was accomplished with stochastic dynamics simulation during 40 ns, using the following protocol: a temperature of 27 °C maintained via stochastic dynamics, integration step of 1 fs, pressure coupling at 1 bar using Berendsen barostat, 18 Å cutoff for the Van-der-Waals interactions. The last 10 ns of the trajectories were used for the analysis. Hydrogen bonds were computed using the program *g_hbond* [24]. Visualization of the results was done in UCSF Chimera [26].

2.4. Umbrella sampling

The calculation of free energy of binding between the Arp2/3 complex in three GMF binding sites was performed using Umbrella sampling. The relaxation of the structural model was performed for 5 ns before the sampling procedure. All titratable amino acids were assigned their canonical state at physiological pH. Next, a molecular mechanics model based on a GROMOS 53a6 force field [27] was constructed. The size of the simulation cell was $210 \times 110 \times 80$ Å^3. The cell was filled with water (model type SPC216). The electroneutrality of the solution was achieved by adding counterions. The simulation of the system was accomplished using the following protocol: a temperature of 27 °C was maintained via stochastic dynamics, integration step of 1 fs, pressure coupling at 1 bar using Berendsen barostat, 14 Å cutoff for the Van-der-Waals interactions. Periodic boundary conditions were applied in all directions. The initial velocities of the atoms were determined by a generator of random numbers on Maxwell distribution. GMF was pulled away from the Arp2/3 complex along the reaction coordinate over 500 ps, using a spring constant of 1000 kJ mol-1 nm-2 and a pull rate of 0.01 nm ps-1 (0.1 Å ps-1). The length of trajectories for a set of statistics was 6–10 ns. Analysis of results was performed using weighted histogram analysis [28]. Multiple sequence alignment was performed with Muscle [21].

3. Results

3.1. Analysis of the interactions in the GMF-IX binding site

First, we analyzed the interactions of the Arp2/3 complex with GMF in the existing crystal structure (binding site GMF-IX). The surface contact between the Arp2/3 complex and GMF in the crystal structure is broad ~1360 Å^2 (Fig. 1A). Analysis of surface contacts in the hydrophobic-hydrophilic representation (Table 1) revealed the presence of a hydrophobic interface between GMF and Arp2/ARPC1 subunits of Arp2/3. The amino acids responsible for hydrophobic interactions are listed in Table 2. Several of these hydrophobicity positions were conservative in other organism Arp2 sequences (Supplementary 1, Fig. S2).

Hydrophobic interactions were supplemented by hydrogen bonds (Fig. 2A and B) between GMF, Arp2 and ARPC1 subunits, that form a dense net (Table 2). Van-der-Waals interactions occur between Val133 and Trp131 in the ARPC1 and the aliphatic portion of Arg64 and Lys97 in GMF. Trp131 packs against the backbone of residues 95–97 in GMF. A comparison to the open Arp2/3 complex [5] reveals the change of rotamers in Trp131 upon binding the GMF, thus allowing the favorable interactions described above and preventing a steric clash between Trp131 and Lys97 in the GMF [12].

The MD simulation confirms that the GMF-IX binding site is stable (Supplementary 2). It revealed a decrease in the number of hydrogen bonds between Arp2, ARPC1 subunits and the GMF (13–8) (Table 2). The center of mass of GMF shifts by ~5.8 Å during the first 20 ns towards the Arp2 subunit (video S1). This movement of GMF led to the formation of new cation-pi interactions (Fig. 2 C, D), thus contributing to the stability of an inactive Arp2/3 conformation. The strongest bonds in the complex preserve during MD simulation and hydrogen bonds GMF with the ARPC1 subunit (Table 2). Several residues with new hydrogen bonds between Arp2 and ARPC1 subunits and GMF are almost strictly conserved (Supplementary 1, bold in Table 2).

Supplementary video related to this article can be found at https://doi.org/10.1016/j.bbrc.2018.01.080.

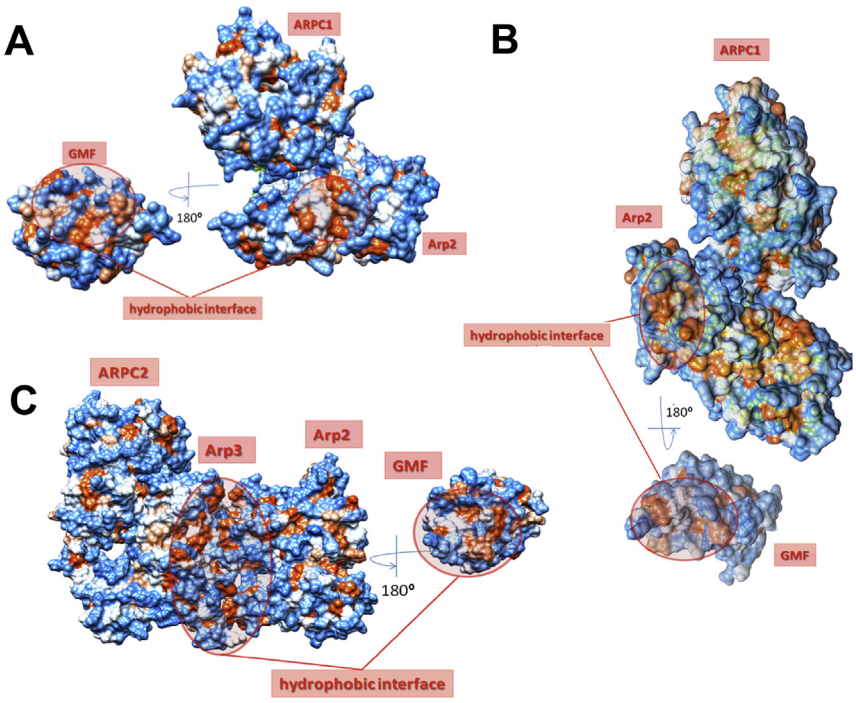

Fig. 1. The surface of the intersubunit contacts of the Arp2/3 complex with the GMF in the hydrophobic-hydrophilic representation in the following binding sites: (A) GMF-IX; (B) GMF-IEM; (C) GMF-IIEM. Hydrophobic regions are colored red and the hydrophilic regions are colored blue. GMF is deployed at 180°. (For interpretation of the references to color in this figure legend, the reader is referred to the Web version of this article.)

Table 1
Hydrophobic surfaces in three binding sites of GMF to Arp2/3 complex.

GMF-IX			GMF-IEM			GMF-IIEM			
GMF	*Arp2*	*ARPC1*	*GMF*	*Arp2*	*ARPC1*	*GMF*	*Arp3*	*ARPC2*	*Arp2*
Leu5	Tyr137	Trp131	Leu5	Ile291	Trp131	Leu5	Val158	Tyr137	Ile40
Val7	Leu 144		Val7	Val329		Val7	Tyr184	Leu144	Leu199
Phe90	Tyr147		Phe21			Phe21	Ile309	Tyr147	Val273
Ser92	Ala148		Phe23			Phe23	Val367	Ala148	
Lys97	Leu 152		Phe90			Leu86	Ile368	Leu152	
Pro98	Val360		Ser92			Phe90	Phe414	Val360	
Met102	Leu361		Lys97			Ser92	Val416	Leu361	
Met103	Ile364		Pro98			Lys97		Ile364	
Ala105	Met365		Met102			Pro98		Met365	
	Phe371		Met103			Met102		Phe371	
			Ala105			Met103			
			Phe 140			Ala105			
						Val120			
						Phe121			
						Ala139			
						Phe140			

3.2. Analysis of the interactions in the GMF-IEM binding site

To study the interactions in the GMF-IEM binding site, we build a molecular model by fitting GMF and Arp2/3 crystal structures into a 3D-EM map of the Arp2/3-Gmf complex in open conformation [14]. There, the additional mass was located close to the Arp2 subunit (yellow arrow on Fig. S1). The contact surface in the GMF-IEM binding site was significantly smaller than in the X-ray structure ~445 Å^2 (Fig. 1B). This may reveal some flattening of the EM structure under negative stain. GMF, Arp2 and ARPC1 subunits all have hydrophobic cavities framed by loops and beta-sheets. These cavities may form the GMF-IEM binding site between the α1-helix, α1-β1-loop of GMF and α10-α11, α13-α14 helixes of Arp2 (Table 2). Analysis of the contact surface revealed the presence of a hydrophobic interface between GMF and the Arp2 subunit (Fig. 3A and B). Several hydrophobic interactions were detected, as well as hydrogen bonds (Table 2).

After MD, new hydrogen bonds between the Arp2 subunit and GMF were formed: Lys336-Tyr84, and, as an example, the double bond between Lys20 = Asp292 (Fig. 3 C, D) et al. Additionally, the new ion pair between GMF and the ARPC1/Arc40 subunit and hydrophobic interactions appeared (Table 2). The GMF center of mass shifted by ~3.9 Å towards the Arp2 subunit during the first 20 ns (video S2). We noticed that residue Asp292 with new hydrogen bonds between Arp2 and GMF is almost strictly conserved (Supplementary 1).

Supplementary video related to this article can be found at https://doi.org/10.1016/j.bbrc.2018.01.080.

Table 2
The residues involved in interactions between GMF and Arp23 complex, identified before and after MD (the residues, involved in interactions after 15–20 ns and the residues, involved in new interactions at last 5 ns MD simultaneously are green, the residues, involved in new interactions at last 5 ns MD are yellow, the conserved residues are bold).

GMF-IX						GMF-IEM						GMF-IIEM					
Before MD			*After MD*			*Before MD*			*After MD*			*Before MD*			*After MD*		
GMF	Arp2	ARPC1	GMF	Arp2	ARPC1	GMF	Arp2	ARPC1	GMF	Arp2	ARPC1	GMF	Arp3	Arp2	GMF	Arp3	Arp2
Hydrophobic interactions						**Hydrophobic interactions**						**Hydrophobic interactions**					
L5	**Y137**	**W131**	L5	**Y137**	**W131**	F23	**Y325**	ND	P12	K336	**W131**	R81		**E75**	F140	**Y184**	**I194**
V7	L144		V6	**A139**		K25	**K339**		Y35								
P98	**Y147**		V7	**V143**					M42								
M102	A148		V94	L144													
M103	L152		P98	**Y147**													
A105	I291		M102	A148													
F140	V360		M103	L152													
	L361		A105	V360													
	I364			L361													
	M365			**I364**													
	F371			**M365**													
				F371													
Salt bridges						**Salt bridges**						**Salt bridges**					
D3	R120	E128	E9	E296	D130	K20	**D292**	ND	E13	**E230**	E50	R81	**E182**	**E75**	K15	E160	R80
K35	E171	D130	E63	**K368**	**K135**	R22	**R294**		K15	**D292**	**R74**	K137	**K317**		R19	E182	H269
K38	**D292**	**K135**	K97	R384	K174	E26	E335		K20	K331	**R97**	E136			K25	**D310**	**E274**
E63	E296		R124						R22	E335	**E126**				D79	**R313**	
R67	K299								K25	**K341**	E128				E116	K317	
K97	H300								E26	**D346**	K174				K119		
K108	**K341**								K74	**R349**	E175				R124		
E122	**R343**								D79	H352					E136		
R124	E345								R110						K137		
E128	**K388**								E116								
K137																	
Hydrogen bonds						**Hydrogen bonds**						**Hydrogen bonds**					
V7	**R149**	**R74**	D3	**N26**	D19	R24	**Y325**	ND	E13	K331	E126	R81		**E75**	D3	G159	R80
K38	**T153**	**E126**	E9	**F27**	T21	K25	**K336**		K15	E335	E128				K15	E160	**D183**
Q41	E296	E128	K38	Y137	Q22				K20	K336	N129				R22	**D310**	H269
Q65	K299	**N129**	Q41	**Y147**	H30				R22	S338	K174				K25	**R313**	**N272** V273
S92	E345	D130	Q44	**N149**	**Y35**				K25	**K339**	E175				D79	Q392	**E274**
G95	**D346**	**W131**	E63	**G150**	E36				E26	**K341**					R80		G275
K97	K368		R64	L152	Q44				M42						V82		
Q100			Q65	**E242**	E47				E48						Y84		
K108			C96	**S243**	Q127				Q50						Q113		
N109			K97	**T245**	E128				D79						E116		
E122			E99	**H300**	**N129**				S83						K119		
R124			Q100	**R349**	E175				Y84						R124		
K137			Q101	**I364**					R110						W133		
			Y104	**M365**					E116						E136		
			R124	K368					A139						K137		
				N370													
				W372													

3.3. Analysis of the interactions in the GMF-IIEM binding site

To build a second EM-derived model we performed a rigid fitting of GMF and Arp2/3 crystal structures into a 3D-EM map of the Arp2/3-Gmf complex in a 'new' open conformation (additional mass at the back of Arp3) [14] (Fig. S1). Analysis of the contact surface in the hydrophobic-hydrophilic representation revealed the presence of a hydrophobic interface formed by the GMF, Arp2 and Arp3 (Fig. 1C). The surface of the contact between the Arp2/3 complex and GMF was ~358 Å^2. Hydrophobic surfaces were supplemented by hydrogen bonds and a double salt bridge (Table 2). These interactions may form a GMF-IIEM binding site between the β3-β4-loop (GMF), α5/α6-helixes (GMF) and β5-α2-loop (Arp2), α15-helix (Arp3) (Fig. 4A). The correlation coefficient of docking this new model into the EM density map using UCSF Chimera increased and became 0.98 after MD.

Analysis of MD trajectories in this site revealed an increase of the number of hydrogen bonds between the Arp2/3 complex and GMF. New hydrogen bonds were formed between GMF and the Arp3 subunit (for example: a double bond between Lys317(ARP3)-Glu136(GMF)-Arg313(ARP3)) and the GMF-Arp2 subunit (Fig. 4B and C). Eight new ion pairs between GMF and the Arp2/3 complex emerged. The GMF center of mass shifts by ~2.2 Å along the Arp2/3 complex during the first 20 ns (video S3). The analysis of multiple alignments revealed conserved residues with new hydrogen bonds between subunits Arp2, Arp3 and GMF after MD (Supplementary 1).

Supplementary video related to this article can be found at https://doi.org/10.1016/j.bbrc.2018.01.080.

3.4. Sequence analysis of subunits, involved into formation of GMF-IIEM binding site

We analyzed the conservation of residues in Arp2 and Arp3 identified in MD simulations as forming salt bridges with GMF (Supplementary 1, 2). The results are presented in Figs. S2 and S3.

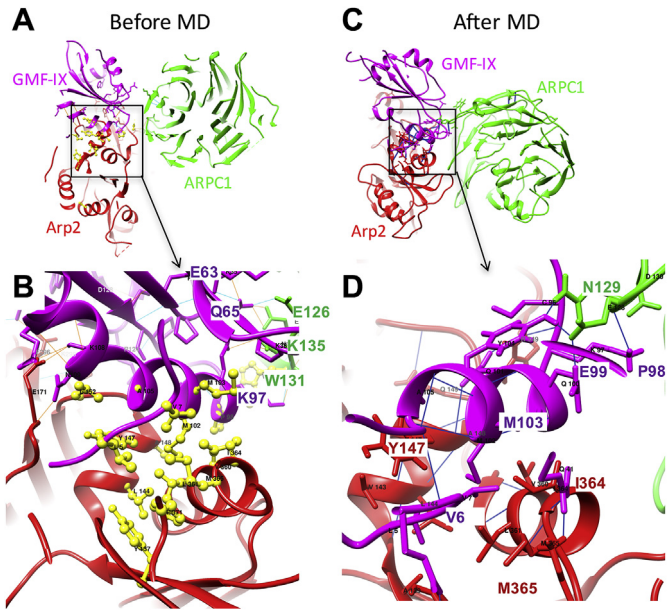

Fig. 2. The contacts between the GMF and the Arp2/3 complex in the GMF-IX binding site. (A) Before MD, (C) after MD, (B, D) enlargement of the contact area.

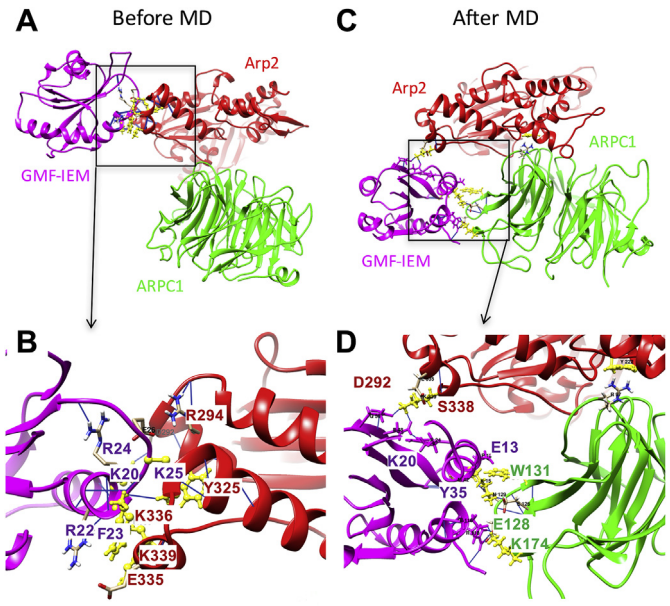

Fig. 3. The contacts between the GMF and the Arp2/3 complex in the GMF-IEM binding site. (A) Before MD, (C) after MD, (B, D) enlargement of the contact area.

Glu160 is located in the variable loop which has various length and sequence in different clades. The top clade containing animals and fungi (orange bar, branch support - 51) contains 6–8 conserved residues, the plant clade (green bar, branch support - 100) is shorter, has different conversed sequences (4 residues in most sequences), and, in the less conserved bottom clade, longer sequences are poorly conserved. Glu182 is frequently replaced with aspartate, but almost no other replacements are observed (except for the asparagine in two plant sequences). Asp310 was found to be absolutely conserved, Arg313 almost conserved, but in some species it is replaced with lysine, and Lys317 is conserved in all top parts of the tree, except *Drosophila melanogaster, Caenorhabditis elegans, Schistosoma mansoni* and *Saccharomyces cerevisiae*, but is

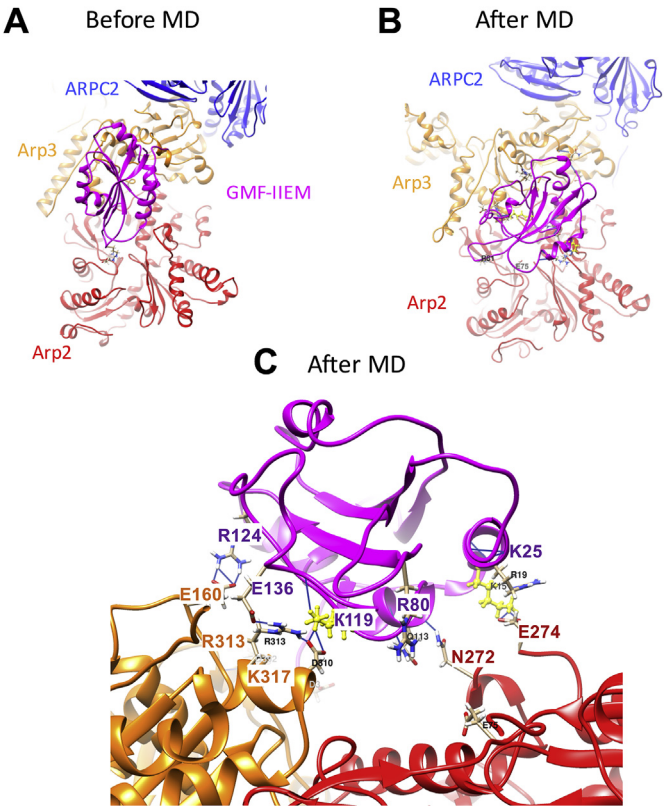

Fig. 4. Contacts between the GMF and the Arp2/3 complex in the binding site GMF-IIEM. (A) Before MD, (B) after MD (C) enlargement of the contact area; complex is rotated 90°, compared to the complex in (B).

replaced with various residues in the less conserved bottom part of the tree.

3.5. Calculation of the free binding energy

The free energy of the GMF binding with the Arp2/3 complex in all binding sites was calculated using Umbrella sampling [29]. At a distance of ~3.8 nm (403 frames) no further interactions between GMF and the Arp2/3 complex in site GMF-IX were detected. The calculated value for the free binding energy of GMF to the Arp2/3 complex at this site was 79 kcal/mol (330.5 kJ/mol). This value corresponds to the breaking of all eight hydrogen bonds, which remained after 10 ns of MD.

Similarly, the free binding energy has been calculated for two EM binding sites. Both low-affinity EM binding sites possess lower free binding energy (62 kcal/mol for GMF-IEM binding site and 45 kcal/mol for GMF-IIEM binding site), probably due to tight interactions in crystal. Additionally, the solvent has an influence on binding of proteins [30].

4. Discussion

Recently, several research groups [5,10,13] with the help of various biochemical and biophysical methods demonstrated that the C-terminus of NPF binds to the Arp2/3 complex at a ratio of 2:1, indicating the presence of two binding sites with different affinity to NPFs: site 1, between Arp2 and ARPC1, that has a higher affinity to NPF [31], and low affinity site 2 on Arp3, close to ARPC3.

The crystal structure of an open Arp2/3 complex with bound GMF [12] uncovered the basics of Arp2/3 complex inhibition. According to this structure, GMF binds to the Arp2/3 complex at the

barbed end of Arp2 and competes with the NPFs for site 1 [5]. The structure of GMF bound to site 2 has not been demonstrated until recently [14]. We recently solved the 3D structure of the Arp2/3 complex with a bound Gmf1 in both sites. Unfortunately, the obtained resolution (22 Å) was not enough to reveal the exact contacts of GMF with Arp2/3, thus the steered MD simulation was used here to predict them. We conducted a structural and dynamic analysis of Arp2/3 complex interactions with GMF in binding sites 1 and 2 and characterized the corresponded hydrophobic interfaces (Fig. 1). Also, the quantitative and qualitative changes in hydrogen bonds in the GMF-Arp2/3 complex have been demonstrated in the course of the MD (Table 2).

To validate the EM data by the X-ray crystallography, we first performed MD simulations and analyzed trajectories for the Arp2/3-GMF crystal structure [12]. This analysis revealed a decrease in the number of hydrogen bonds between the GMF, Arp2 and ARPC1 subunits after MD of the complex. Interestingly, after MD, the GMF center mass was offset by 1 Å on the z-axis towards the Arp2 subunit (video S1). This suggests that the interactions revealed in the crystal structure are dynamic. Next, we analyzed the MD trajectories of the Arp2/3 complex with GMF at the binding sites revealed by single particle EM: GMF-IEM (Fig. 3) and GMF-IIEM (Fig. 4). We detected an increase in the number of hydrogen bonds between the GMF and the Arp2/3 complex in both sites after MD. This suggests that interactions in both EM-determined sites were determined correctly. The majority of hydrophobic-hydrophilic interactions were detected in the binding site GMF-IEM, which is consistent with it being a high-affinity binding site 1.

It is interesting to note that the initially distant positions of GMF relative to Arp2 in GMF-IX and GMF-IEM sites shifted after MD towards each other to roughly the same position. This is supported by the fact that the identified key interacting residues at site 1 are the same in both structures, solved by X-ray crystallography and single particle EM: W131, E128 (Table 2). However, the evaluation of the potential profile of moderate strength demonstrated that these structures differ in GMF binding energy: 79 kcal/mol for GMF-IX versus 62 kcal/mol for GMF-IEM.

The binding site GMF-IIEM (site 2) does not have a crystal analogue. So we positioned the GMF into a difference density, obtained by subtracting 3D-EM structures of Arp2/3-GMF [14] and the Arp2/3 complex [32]. This volume was large enough to roughly fit the GMF monomer at the back of the Arp3 subunit (Fig. S1). After MD, this newly identified binding site demonstrated a good position of GMF, with balanced salt bridges and a hydrophobic environment. The binding site for GMF is formed by residues Glu160, Asp310, Arg313, Lys317 of the Arp3 subunit and residues Asn272 and Glu274 of the Arp2 subunit (Fig. 4C). No interactions of GMF with the Arp2 subunit were identified before. The number of formed salt bridges between GMF and the Arp2/3 complex was fewer than for site 1 (Table 2), suggesting that this site has a lower affinity to GMF. Accordingly, the free binding energy of GMF in this site was lower, 45 kcal/mol.

Finally, we looked deeper into the phylogenic origin of the amino acids in Arp3 and Arp2 subunits that form a newly identified binding site for GMF. We searched for homologues of chain A (Arp3) and B (Arp2) from the bovine Arp2/3 complex (pdb id 4JD2) in a representative sample of 84 eukaryotic genomes (see Table S1 for a complete list). The specific amino acid residues in GMF that interact with the Arp2/3 complex in both binding sites specified by MD simulations are conserved throughout all homologues from evolutionarily distant species (Figs. S3 and S4). This suggests the universality of the molecular mechanisms of interaction of the Arp2/3 complex with GMF in binding site 2.

Together, crystal structures fitting, EM and homology modeling approaches allowed us to make complementary and testable predictions about the specific Arp2/3 complex surface residues that are involved in interactions with GMF in two binding sites. These findings may now be used to characterize the binding of other Arp2/3 complex inactivators in two above-mentioned sites.

Acknowledgments

Authors would like to thank Ms Lisa Trifonova for proofreading the manuscript. MD studies were supported by the RSF (14-14-00234 to O.S.); bioinformatics analysis was supported by the RFBR (16-34-60252 to A.P.); D.D. was supported by grant to V.A.Sadovnichiy from the RSF (14-50-00029). Simulations were performed at Supercomputer Centers: “Arian Kuzmin” (NEFU), “Lomonosov” (MSU) and “Complex for simulation and data processing for mega-science facilities” (NRC “Kurchatov Institute”).

Appendix A. Supplementary data

Supplementary data related to this article can be found at https://doi.org/10.1016/j.bbrc.2018.01.080.

Transparency document

Transparency document related to this article can be found online at https://doi.org/10.1016/j.bbrc.2018.01.080.

References

[1] I. Dang, R. Gorelik, C. Sousa-Blin, et al., Inhibitory signalling to the Arp2/3 complex steers cell migration, Nature 503 (2013) 281–284, https://doi.org/10.1038/nature12611.
[2] X. Chi, S. Wang, Y. Huang, et al., Roles of rho GTPases in intracellular transport and cellular transformation, Int. J. Mol. Sci. 14 (2013) 7089–7108, https://doi.org/10.3390/ijms14047089.
[3] Z. Chen, D. Borek, S.B. Padrick, et al., Structure and control of the actin regulatory WAVE complex, Nature 468 (2010) 533–538, https://doi.org/10.1038/nature09623.
[4] M.-F. Carlier, M. Hertzog, D. Didry, et al., Structure, function, and evolution of the beta-Thymosin/WH2 (WASP-Homology2) actin-binding module, Ann. N. Y. Acad. Sci. 1112 (2007) 67–75, https://doi.org/10.1196/annals.1415.037.
[5] S.-C. Ti, C.T. Jurgenson, B.J. Nolen, T.D. Pollard, Structural and biochemical characterization of two binding sites for nucleation-promoting factor WASp-VCA on Arp2/3 complex, Proc. Natl. Acad. Sci. U. S. A. 108 (2011) E463–E471, https://doi.org/10.1073/pnas.1100125108.
[6] T.D. Pollard, Regulation of actin filament assembly by Arp2/3 complex and formins, Annu. Rev. Biophys. Biomol. Struct. 36 (2007) 451–477, https://doi.org/10.1146/annurev.biophys.35.040405.101936.
[7] J.-F. Gaucher, C. Maugé, D. Didry, et al., Interactions of isolated C-terminal fragments of neural Wiskott-Aldrich syndrome protein (N-WASP) with actin and Arp2/3 complex, J. Biol. Chem. 287 (2012) 34646–34659, https://doi.org/10.1074/jbc.M112.394361.
[8] A.E. Kelly, H. Kranitz, V. Dötsch, R.D. Mullins, Actin binding to the central domain of WASP/Scar proteins plays a critical role in the activation of the Arp2/3 complex, J. Biol. Chem. 281 (2006) 10589–10597, https://doi.org/10.1074/jbc.M507470200.
[9] X.-P. Xu, I. Rouiller, B.D. Slaughter, et al., Three-dimensional reconstructions of Arp2/3 complex with bound nucleation promoting factors, EMBO J. 31 (2012) 236–247, https://doi.org/10.1038/emboj.2011.343.
[10] M. Boczkowska, G. Rebowski, D.J. Kast, R. Dominguez, Structural analysis of the transitional state of Arp2/3 complex activation by two actin-bound WCAs, Nat. Commun. 5 (2014) 3308, https://doi.org/10.1038/ncomms4308.
[11] C.A. Ydenberg, S.B. Padrick, M.O. Sweeney, et al., GMF severs actin-arp2/3 complex branch junctions by a cofilin-like mechanism, Curr. Biol. 23 (2013) 1037–1045, https://doi.org/10.1016/j.cub.2013.04.058.
[12] Q. Luan, B.J. Nolen, Structural basis for regulation of Arp2/3 complex by GMF, Nat. Struct. Mol. Biol. 20 (2013) 1062–1068, https://doi.org/10.1038/nsmb.2628.
[13] S.B. Padrick, L.K. Doolittle, C.A. Brautigam, et al., Arp2/3 complex is bound and activated by two WASP proteins, Proc. Natl. Acad. Sci. U. S. A. 108 (2011) E472–E479, https://doi.org/10.1073/pnas.1100236108.
[14] O.S. Sokolova, A. Chemeris, S. Guo, et al., Structural basis of Arp2/3 complex inhibition by GMF, coronin, and arpin, J. Mol. Biol. 429 (2017) 237–248, https://doi.org/10.1016/j.jmb.2016.11.030.
[15] A.A. Rodal, O. Sokolova, D.B. Robins, et al., Conformational changes in the Arp2/3 complex leading to actin nucleation, Nat. Struct. Mol. Biol. 12 (2005) 26–31, https://doi.org/10.1038/nsmb870.

[16] T.V. Pyrkov, A.O. Chugunov, N.A. Krylov, et al., PLATINUM: a web tool for analysis of hydrophobic/hydrophilic organization of biomolecular complexes, Bioinformatics 25 (2009) 1201–1202, https://doi.org/10.1093/bioinformatics/btp111.
[17] K.G. Tina, R. Bhadra, N. Srinivasan, PIC: protein interactions calculator, Nucleic Acids Res. Web Serv. 35 (2007) 473–476, https://doi.org/10.1093/nar/gkm423.
[18] L.C. Xue, J.P. Rodrigues, P.L. Kastritis, et al., PRODIGY: a web server for predicting the binding affinity of protein–protein complexes, Bioinformatics (2016), https://doi.org/10.1093/bioinformatics/btw514 btw514.
[19] S.F. Altschul, W. Gish, W. Miller, et al., Basic local alignment search tool, J. Mol. Biol. 215 (1990) 403–410, https://doi.org/10.1016/S0022-2836(05)80360-2.
[20] N.A. O'Leary, M.W. Wright, J.R. Brister, et al., Reference sequence (RefSeq) database at NCBI: current status, taxonomic expansion, and functional annotation, Nucleic Acids Res. 44 (2016) D733–D745, https://doi.org/10.1093/nar/gkv1189.
[21] R.C. Edgar, MUSCLE: a multiple sequence alignment method with reduced time and space complexity, BMC Bioinf. 5 (2004) 113, https://doi.org/10.1186/1471-2105-5-113.
[22] A.M. Waterhouse, J.B. Procter, D.M.A. Martin, et al., Jalview Version 2–a multiple sequence alignment editor and analysis workbench, Bioinformatics 25 (2009) 1189–1191, https://doi.org/10.1093/bioinformatics/btp033.
[23] S. Kumar, G. Stecher, K. Tamura, MEGA7: molecular evolutionary genetics analysis version 7.0 for bigger datasets, Mol. Biol. Evol. 33 (2016) 1870–1874, https://doi.org/10.1093/molbev/msw054.
[24] S. Pronk, S. Rd, P. Ll, et al., GROMACS 4.5: a high-throughput and highly parallel open source molecular simulation toolkit, 29 (2013) 845–854. https://doi.org/10.1093/bioinformatics/btt055.
[25] G.A. Kaminski, Accurate prediction of absolute acidity constants in water with a polarizable force field: substituted phenols, methanol, and imidazole, J. Phys. Chem. B 109 (2005) 5884–5890, https://doi.org/10.1021/jp050156r.
[26] E.F. Pettersen, T.D. Goddard, C.C. Huang, et al., UCSF Chimera–a visualization system for exploratory research and analysis, J. Comput. Chem. 25 (2004) 1605–1612, https://doi.org/10.1002/jcc.20084.
[27] C. Oostenbrink, A. Villa, A.E. Mark, W.F. van Gunsteren, A biomolecular force field based on the free enthalpy of hydration and solvation: the GROMOS force-field parameter sets 53A5 and 53A6, J. Comput. Chem. 25 (2004) 1656–1676, https://doi.org/10.1002/jcc.20090.
[28] J.D. Chodera, W.C. Swope, J.W. Pitera, et al., Use of the weighted histogram analysis method for the analysis of simulated and parallel tempering simulations, J. Chem. Theor. Comput. 3 (2007) 26–41, https://doi.org/10.1021/ct0502864.
[29] J.A. Lemkul, D.R. Bevan, Assessing the stability of Alzheimer's amyloid protofibrils using molecular dynamics, J. Phys. Chem. B 114 (2010) 1652–1660, https://doi.org/10.1021/jp9110794.
[30] D. Chakravarty, J. Janin, C.H. Robert, P. Chakrabarti, Changes in protein structure at the interface accompanying complex formation, IUCrJ 2 (2015) 643–652, https://doi.org/10.1107/S2052252515015250.
[31] M.O. Sweeney, A. Collins, S.B. Padrick, B.L. Goode, A novel role for WAVE1 in controlling actin network growth rate and architecture, Mol. Biol. Cell 26 (2015) 495–505, https://doi.org/10.1091/mbc.E14-10-1477.
[32] R.C. Robinson, K. Turbedsky, D.A. Kaiser, et al., Crystal structure of Arp2/3 complex, Science 294 (2001) 1679–1684, https://doi.org/10.1126/science.1066333.